





Article

Improvement of the 2007–2015 Earthquake Catalog Along the 300 km Long Postglacial Merasjärvi–Stuoragurra Fault Complex in Northern Fennoscandia Using Automatic Event Detection

Daniela Calle-Gardella ¹, Claudia Pavez-Orrero ^{2,3,*}, Diana Comte ^{1,4}, Felix Halpaap ⁵, Odleiv Olesen ⁶, Alina Espinoza ^{1,4} and Steven Roecker ⁷

¹ Advanced Mining Technology Center, Facultad Ciencias Físicas y Matemáticas, Universidad de Chile, Santiago P.O. Box 8370451, Chile; daniela.calle@amtc.cl (D.C.-G.); dcomte@dgf.uchile.cl (D.C.); alina.espinoza@ug.uchile.cl (A.E.)

² Department of Physics, Faculty of Sciences, Universidad de Tarapacá, Arica P.O. Box 1010069, Chile

³ SINTEF Industry, P.O. Box 4760 Torgarden, NO-7465 Trondheim, Norway

⁴ Departamento de Geofísica, Facultad Ciencias Físicas y Matemáticas, Universidad de Chile, Santiago P.O. Box 8370449, Chile

⁵ Department of Earth Science, University of Bergen, NO-5007 Bergen, Norway; felix.halpaap@uib.no

⁶ Norges Geologiske Undersøkelse, NO-7491 Trondheim, Norway; odleiv.olesen@ngu.no

⁷ Earth and Environmental Sciences, School of Science, Rensselaer Polytechnic Institute, Troy, NY 12180, USA; roecks@rpi.edu

* Correspondence: claudia.pavez.orrego@sintef.no

Abstract: We present an updated and validated seismic catalog for the northern Fennoscandian region, focusing on postglacial faults from the Merasjärvi fault system in the southwest to the Iešjávri fault system in the northeast. This work involved a comprehensive review of continuous waveforms derived from open datasets from 2007 to 2015 and processed using the Regressive ESTimator algorithm. The primary objective was to refine the delineation of seismicity along the above-mentioned postglacial faults and highlight their seismic potential. Our analysis revealed distinct waveform patterns originating primarily from two main sources: approximately 15% were associated with areas mapped as postglacial faults, and the remainder of the events outside these areas, 89%, were concentrated in areas with active mines. Compared to previously reported events in the Fennoscandian Earthquake Catalogue (FENCAT), we observed a 22% increase in seismic activity within postglacial fault zones. These results demonstrate that the Regressive ESTimator algorithm not only improves the detection of tectonic seismicity but also effectively identifies seismic signals resulting from mining activities in the study area. The Merasjärvi, Lainio–Suijavaara, Palojärvi, and Maze and Iešjávri fault systems appear to form a continuous deformation complex of approximately 300 km long, which we propose naming the Merasjärvi–Stuoragurra fault complex.

Keywords: postglacial faults; northern Fennoscandia; Stuoragurra fault; Maze and Iešjávri fault; Palojärvi fault; Lainio–Suijavaara fault; Merasjärvi fault



Citation: Calle-Gardella, D.; Pavez-Orrero, C.; Comte, D.; Halpaap, F.; Olesen, O.; Espinoza, A.; Roecker, S. Improvement of the 2007–2015 Earthquake Catalog Along the 300 km Long Postglacial Merasjärvi–Stuoragurra Fault Complex in Northern Fennoscandia Using Automatic Event Detection. *Geosciences* **2024**, *14*, 293. <https://doi.org/10.3390/geosciences14110293>

Academic Editor: Riccardo Caputo

Received: 4 September 2024

Revised: 23 October 2024

Accepted: 24 October 2024

Published: 1 November 2024



Copyright: © 2024 by the authors. Licensee MDPI, Basel, Switzerland. This article is an open access article distributed under the terms and conditions of the Creative Commons Attribution (CC BY) license (<https://creativecommons.org/licenses/by/4.0/>).

1. Introduction

Isostatic adjustment is a geological faulting mechanism in which faults are caused or reactivated by glacially induced isostatic stresses released during or after ice sheet melting [1]. These types of faults are usually referred to as postglacial faults (PGFs) or glacially induced faults (GIFs), depending on the reference to the general mechanism or the reactivated structures [1]. The PGFs have been observed in several locations around the world, such as the Fennoscandian Shield [2–11], Denmark [12–14], Germany [15,16], Poland [17,18], Canada [19,20], and Alaska [21,22]. They are predominantly located in intraplate zones, although some have been observed at plate boundaries [1].

PGFs in Fennoscandia have been accompanied by large earthquakes with moment magnitudes ranging from 6 to 8, scarp heights of a few meters, and fault lengths of over a hundred kilometers [4,6,23,24]. These earthquakes generate landslides and/or soft-sediment deformation structures (SSDSs) [1]. Most of these structures remain seismically active [24].

One of the main concerns of the seismological community regarding the PGFs in the area is the lack of regional geophysical studies and imaging, which makes it difficult to demonstrate any kind of subsurface geological connection. Nordic countries such as Norway, Finland, and Sweden are very interested in gaining a new understanding of the complexity behind the PGFs. In this sense, many techniques have been used recently to discover new faults or to improve the existing knowledge (LiDAR [25]; landslide dating [26]; fault dating [24,27]).

The present study aimed to improve the current understanding of PGFs in northern Fennoscandia, focusing on the Merasjärvi, Lanio–Suijavaara, Palojärvi, and Maze and Iešjávri fault systems. This was achieved by reprocessing open-access seismological records from stations installed in the region, in order to increase the detection rate of earthquake events and generate an updated seismic catalog. With this revised catalog, we provide a clearer perspective on the seismicity distribution in the area, and a better understanding of how it is influenced by the fault systems. Additionally, the reprocessing of seismological data in this study helped to identify seismicity associated with human activities, such as oil and gas extraction and mining operations [28,29]. In particular, mining is an important activity in northern Fennoscandia [30], so this study aimed to improve the description of earthquakes associated with different mining sources located in the area. This distinction could help to improve the earthquake coverage for future tomographic studies.

2. Geotectonic and Seismological Framework

2.1. Northern Fennoscandia Geotectonics

During the last stages of the Weichselian glaciation (~15,000–9000 years B.P.), the reduction in ice loads induced a rapid uplift in Fennoscandia. This resulted most likely in active faulting of the bedrock in northern Fennoscandia, with the occurrence of large-magnitude earthquakes [2,23,24,31–34]. The faults that arose through this process were originally called PGFs or GIFs, even though radiocarbon dates indicate that some of them were formed during and before glaciation and other scarps long after deglaciation.

Many factors are currently contributing to the stress field in northern Fennoscandia, which may be additionally responsible for the faulting development. Multiple investigations suggest that the lithosphere in northern Fennoscandia is building up elastic strain over long periods of time. Some of the main commonly accepted stress-generating mechanisms are (i) gravitational potential energy changes produced due to topographic loads, (ii) post-glacial isostatic adjustments, which seem to have a larger role in northern Fennoscandia than in the southern part, (iii) mid-Atlantic ridge push, (iv) Quaternary glacial erosion, and (v) flexural stresses through sedimentation. Among these tectonic stress sources, the ridge push from the NE Atlantic spreading, whose velocity at the Knipovich segment has varied significantly during the last 12 Ma [35], arises as one of the main mechanisms. Gradual and transient stress perturbations such as erosion, fluid migration, and anthropogenic effects can also trigger faulting, contributing to the seismicity rates [36–39]. Most of the observed faults are reverse and low-angle thrusts dipping to the southeast, indicating compressional forces related to tectonic wrenching [40]. In situ stress measurements show that the maximum principal stress is compressional and essentially horizontal [40].

From the geological context, it is possible to infer that some of the PGFs in northern Fennoscandia are related to the reactivation of pre-existing zones of weakness through as-yet-unknown mechanisms, even though GIA (glacial isostatic adjustment) is triggering local reactivations [1]. Therefore, at present, we cannot know with certainty which faults and fault segments were reactivated at which time and due to which mechanism.

PGFs with very clear surface expressions can be found in at least 14 localities around Fennoscandia (red lines in Figure 1), including northern Finland, Sweden, and Norway [41–43]. These faults are the only confirmed and well-characterized at the km scale in the world [4,42,44], ranging between 2 and 160 km long with vertical displacements of up to 30 m [41]. The largest are the Pärvie (Sweden) and the Stuoragurra (Norway) faults [4]. Additionally, a set of shorter GIFs—but still seismically active—can be found spread in the region between latitudes 64° and 70° N, as Palojärvi (Finland) [45,46], Lainio–Suijavaara (Sweden) [7,42,47], and Merasjärvi (Sweden) [7,9,42,47]. They generally strike SW–NE, and they are commonly interpreted as thrust faults. Our study was focused on four postglacial fault systems: the Maze and Iešjávri, the Palojärvi, the Lainio–Suijavaara, and the Merasjärvi.

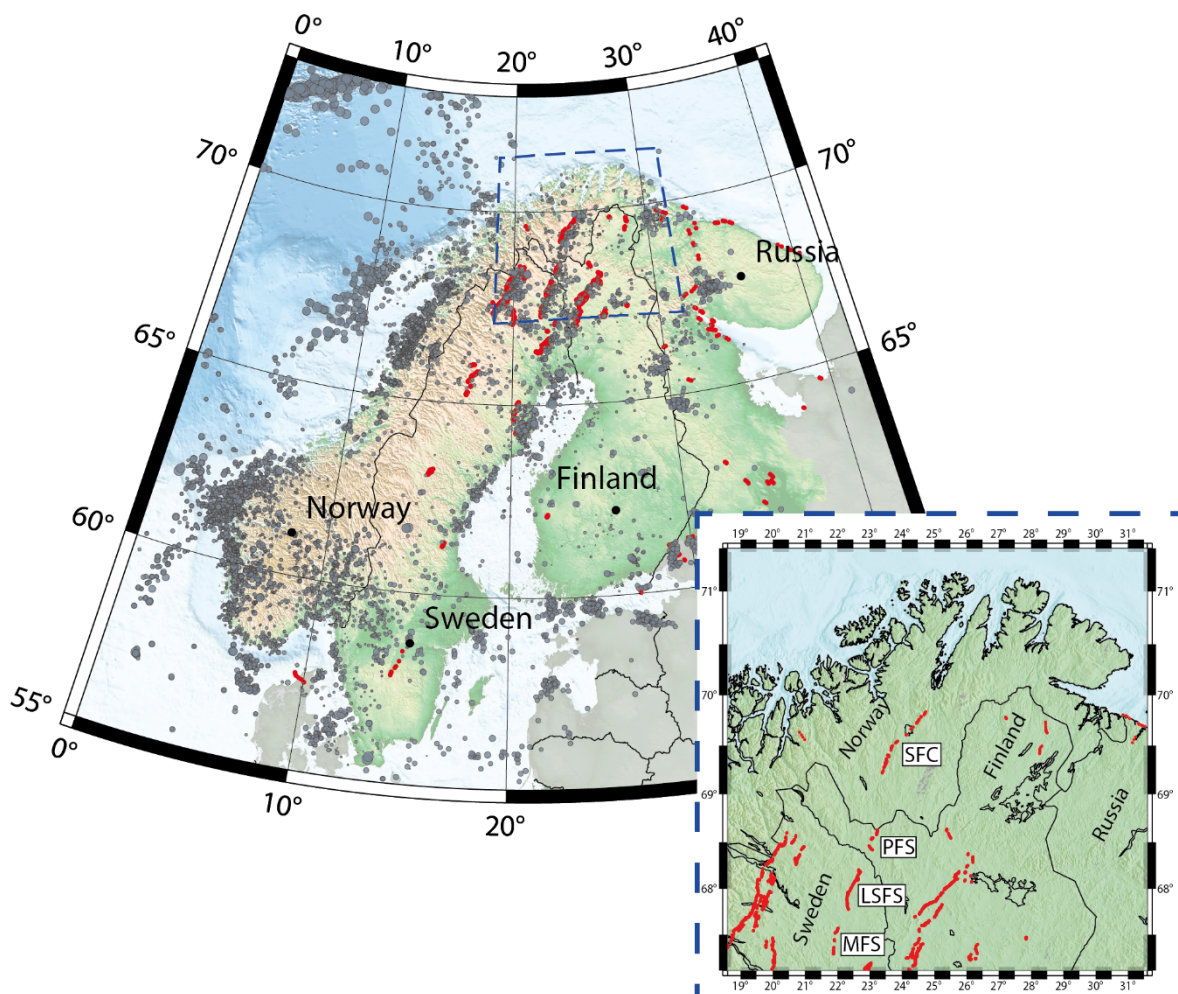


Figure 1. Main postglacial faults in Fennoscandia, outlined with red color. The study area has been demarcated with a dashed blue box. In red, the main PGFs: SFC: Stuoragurra fault complex; PFS: Palojärvi fault system; LSFS: Lainio–Suijavaara fault system; MFS: Merasjärvi fault system.

2.1.1. Maze and Iešjávri Fault System (MIFS)

The Maze and Iešjávri fault system, with a total length of c. 90 km, constitutes the Norwegian part of the Lapland province of postglacial faults in northern Fennoscandia [24]. Ref. [24] interpreted three fault systems in the fault complex, while [48] recently acquired more data and concluded that the two southernmost systems can be merged into one system. The fault systems have generally been referred to as the Stuoragurra fault complex (SFC) [24,48]. The distance between the Máze fault system to the southwest and the Iešjávri fault system to the northeast is 12 km. The faults dip at angles of 30–75° to the SE and could

be traced in reflection seismic data to a depth of c. 500 m [24]. The faults were originally assumed to be formed during or immediately after deglaciation [36]. Trenching across the fault rupture at nine sites along the fault complex reveals deformed sediments in all sites, and there are inclusions of peat and organic-bearing soil in the deformed and partly overrun loose deposits on the footwall in eight of the sites [24,27,48]. Radiocarbon dating of organic matter located in buried and severely deformed sediment horizons indicates late Holocene ages for the (final) formation of the different fault segments, suggesting that the Máze fault system was formed during an earthquake less than 500 years ago [48], and the Iešjávri fault system was formed less than 4000 years BP [24,48]. According to these dates, some of the faulting occurred around 10,000 years after deglaciation, and they were not an immediate result of the deglaciation rebound. The maximum displacement of the Maze and Iešjávri fault systems are 10 and 4 m, respectively, while the maximum scarp heights are 7 and 3 m for the two systems [4,24]. The lengths of the two systems are 42 and 36 km, respectively, and the magnitudes for the two earthquakes are estimated to be around of 6.8 and 6.9. No strike-slip displacement has so far been observed along the fault. Its shallow segment was previously studied through core drilling and geophysical profiling [4,24]. Earthquakes related to the two fault systems follow a linear spatial distribution along a c. 30 km wide cluster parallel to the fault and below the hanging wall block [23,24,36] with errors less than 30 km in location for small and medium-sized events. The axis of the cluster is displaced approximately 30 km to the southwest of the surface expression of the fault, which seems to be consistent with the fault dip ($\sim 40\text{--}50^\circ$) and the mean depth of the earthquakes (~ 19 km).

2.1.2. Palojärvi Fault System (PFS)

Three main reverse structures comprise the PFS. The first trace corresponds to the main structure, called the Palojärvi fault. This trace is 6 km long, trending NNE-SSW, and with a vertical displacement of around 6.8 m indicated by the fault scarp from the offset. The fault is separated into several secondary parallel structures, which can be observed in the hanging wall block [45]. Considering the vertical offset, the earthquake that gave rise to this fault had an estimated moment magnitude $M_w \sim 7.0$. This fault presents strong signs of fracture reactivation, as oxidized iron minerals have been observed [45].

The second structure, the Paatsikkajoki fault, is 6 km long and oriented to the W-E, bending towards the NE at the east of the structure. The fault scarp is 1.7–2 m high, which translates into an estimated maximum magnitude of $M_w \sim 6.7$ [49]. A second 2 km long segment with a displacement between 0.3 and 1.5 m in height is located 1 km south of the main structure. According to the offset, the formation magnitude was $M_w \sim 6.5$ [45]. This structure seems to have been formed in subaerial conditions, after deglaciation.

The last segment, called the Kultima fault, differs from the others as it trends SE-NW. Its scarp is 30 m at its highest point, which reflects a moment magnitude $M_w > 7.0$. This fault might have been formed by the late glacial isostatic rebound.

2.1.3. Lainio–Suijavaara Fault System (LSFS)

The Lainio–Suijavaara fault is a continuous fault of about 50 km long, accompanied by three shorter fault scarps, each about 2–3 km long, centrally located in front of the main fault. The average scarp heights is between 10 and 20 m. Two-thirds of the fault from the north strikes NNE-SSW, while the southernmost section strikes SSE. The northern part of the fault was formed prior to deglaciation. Some other segments show evidence of postglacial faulting, according to the presence of geological structures that cross-cut the main fault [42,50]. The moment magnitude of the main formation event was estimated at $M_w \sim 7.1$ [14]. Ample groundwater discharge at the fault scarps indicates considerably fractured bedrock in the fault.

2.1.4. Merasjärvi (MFS)

The Merasjärvi fault, located in northern Sweden 25 km south of the LSFS, strikes NNE-SSW and has an approximate length of 8 km. Its scarp maximum height is 15 m,

located in the southern part of the fault [42]. This fault probably originated in two rupture events, although the timing of these ruptures is still not well-understood [50,51]. However, it is known that both ruptures are younger than the Middle Weichselian, as fault scarps indicate that faulting occurred at the end of or after the last deglaciation in the area.

The tectonic connection through regional structures between PGFs is still unknown, as the trace extension of the faults in depth has not been monitored. However, the similar spatial locations and strikes of the PGFs suggest a regional tectonic link between them, even though each individual fault has well-distributed local seismicity (Figure 2). Recent progress in airborne LiDAR (Laser Imaging Detection and Ranging) detection allows the discovery of new potential PGFs, making it possible to better interpret the available seismicity data and structural models. As an example, seismicity maps reveal current deformation between the SFC and the airborne detected PFS in Finland (Figure 1) [45]. The latter is consistent with fault plane solutions, which reveal a strike–slip event between PGFs [23].

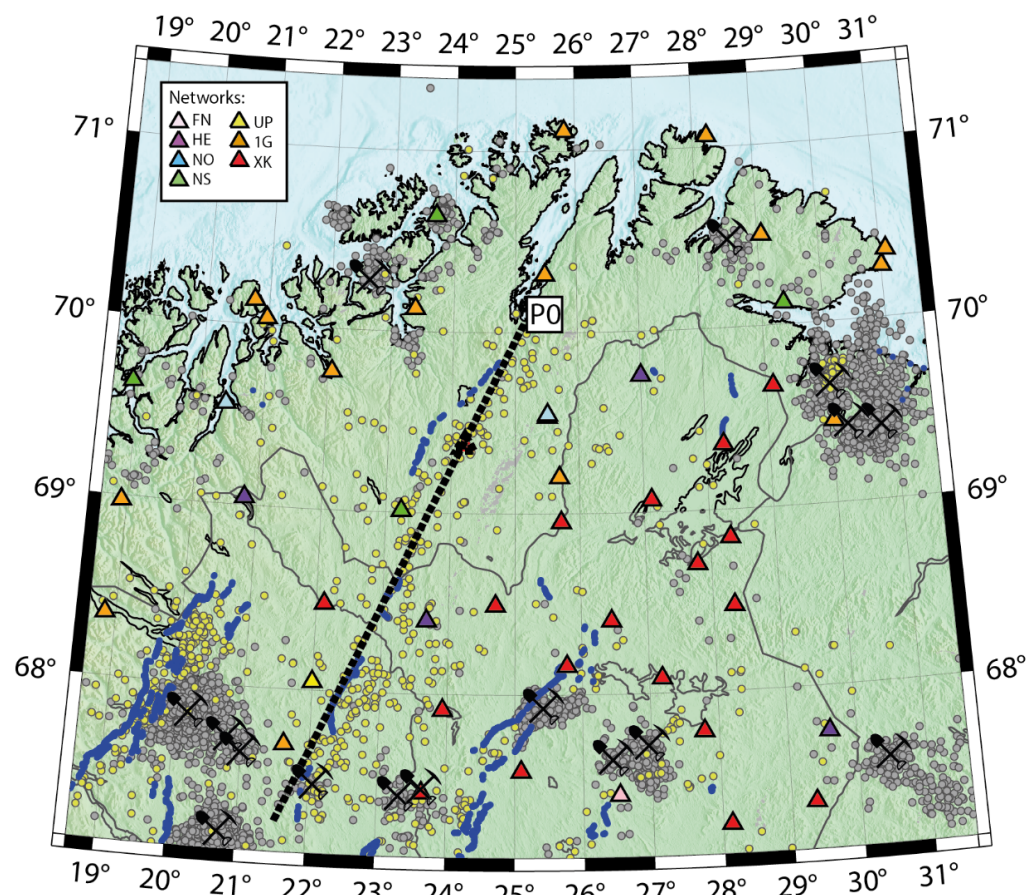


Figure 2. Map of the study area for the period of 2007–2015. Blue lines represent major postglacial faults. Triangles represent the seismic stations used in this study. Stations are color-coded according to the network to which they belong. Shovel cross symbols represent active mines in the study area. Dots represent earthquakes: yellow dots are seismicity reported by FENCAT, and gray dots represent mining events (explosion, induced or triggered events) from NNSN and ISUH bulletins. The black dotted line represents a profile (P0) along the main traces of the PGFs.

2.2. Seismicity in Fennoscandia

The tectonic seismicity in Fennoscandia has been compiled in the Fennoscandian earthquake catalog (FENCAT) by the Institute of Seismology of the University of Helsinki (ISUH) [52]. This seismicity is characterized by low to moderate magnitudes ($M_w \leq 4.0$) and strictly intraplate activity, both onshore and offshore on the passive continental

shelf [4,44]. On the other hand, anthropogenic seismic activity in Fennoscandia represents most of the seismic signals from monitoring centers in the region, such as the Norwegian National Seismic Network (NNSN), ISUH, and Svenska Nationella Seismiska Nätet (SNSN). In the NNSN catalog [53], anthropogenic seismicity (classified by NNSN as explosions, induced or triggered events) represents ~80% of the total. In the case of ISUH, seismicity associated with explosions presented in the latest monthly bulletins from 2009 to 2016 [54] represents ~97% of the records. And in the case of SNSN, [55] described that the recorded events are mainly correlated with anthropogenic seismic activity, whose distribution is dominated by the two underground iron mines in northern Sweden.

Northern Fennoscandia

To form one of the PGFs in northern Fennoscandia during a single seismic event [14] would require an earthquake of $M_w = 6.0\text{--}7.5$ [2,4,24,56]. This contrasts with the present-day intraplate pattern, which is characteristic of a stable continental region, even though such a tectonic setting seems to be necessary for the formation of a glacial fault [57,58]. The earthquake epicenter locations (Figure 1) are correlated with the mapped locations of PGFs [58]. Many earthquakes are distributed in clusters southeast of the fault scarps, in relation to their dip direction [58,59], and with depths varying approximately between 2 and 30 km depth. This distribution of events suggests that PGFs represent relevant tectonic structures at a crustal scale, which are currently seismically active [27,60]. The cause of these increased present-day seismicity levels related to PGFs is still unknown. One hypothesis mentions the static stress change induced by the earthquakes that caused the faults, which would suggest very long lithospheric relaxation times and a very low tectonic stress rate [1]. Other possibilities are the remnants of GIA stresses or tectonic stress [61]. As it is, the accumulated stress is episodically released through high-magnitude—e.g., historical earthquakes—or smaller events, which leads to stress stabilization. However, all the above-mentioned stress mechanisms are consecutively building up a new stress field. It is not known when this stress will be drastically released through a high- or medium-magnitude event.

3. Data and Methods

3.1. The Study Area

The study area was selected with the primary objective of improving the official catalog of these faults and surrounding areas by reprocessing seismological records of the past decade.

To delineate our study area and the time period in which the catalog would be improved, we used as criteria the coverage and distribution of active seismological stations with open records around the faults. In addition, we considered active mines that azimuthally cover the faults and generate seismic activity associated with their production processes:

- Seismological stations: Using the map from the Seismological Facility for the Advancement of Geoscience [62], we searched for all networks installed in the vicinity of the faults and their recording period. Five permanent networks were found: FN [63], HE [64], NO [65], NS [66], and UP [67]. Through the open data centers (GEOFON, IRIS, ORFEUS, RESIF, and UIB-NORSAR), we checked the stations with open and downloadable seismological records. Then, we searched for temporary networks that would support the coverage of the faults and found two temporary networks: XK [68] and 1G [69].

Based on the increased availability of recording stations, the study period was selected as from 2007 to 2015, a timeframe during which both temporary networks were operational.

- Active mines: The history of mining activity in Fennoscandia began more than 2000 years ago. It has been increasing since the end of the Second World War [30]. Currently, more than 100 mines are active in Norway, Finland, and Sweden [30]. In

northern Fennoscandia, large mines are located near the PGFs [70], such as the Lillebukt, Gammasnes, and Bjørnefjell mines in Norway, the Kevitsa and Suurikuusikko (or Kittilä) mines in Finland, and the Kiruna and Malmberget mines in Sweden.

3.2. Official Seismic Catalog

The study area presents natural earthquakes and mining activity (explosions, induced or triggered events), which is shown with gray and yellow dots in Figure 2 (data obtained from the FENCAT catalog [52], NNSN catalog [53], and ISUH bulletins [54]). Given our focus on tectonic earthquakes associated with PGFs, we used the FENCAT catalog as a baseline, which we further refined and expanded in this study (see Supplements S1 and S2).

The natural earthquakes in the official catalogs are low-magnitude and cortical, most of them near faults extending from the SFC to the MFS, and located up to 30 km deep (yellow dots in Figure 3). Mining earthquakes are shallow, most of them located at the near-surface (gray dots in Figure 3).

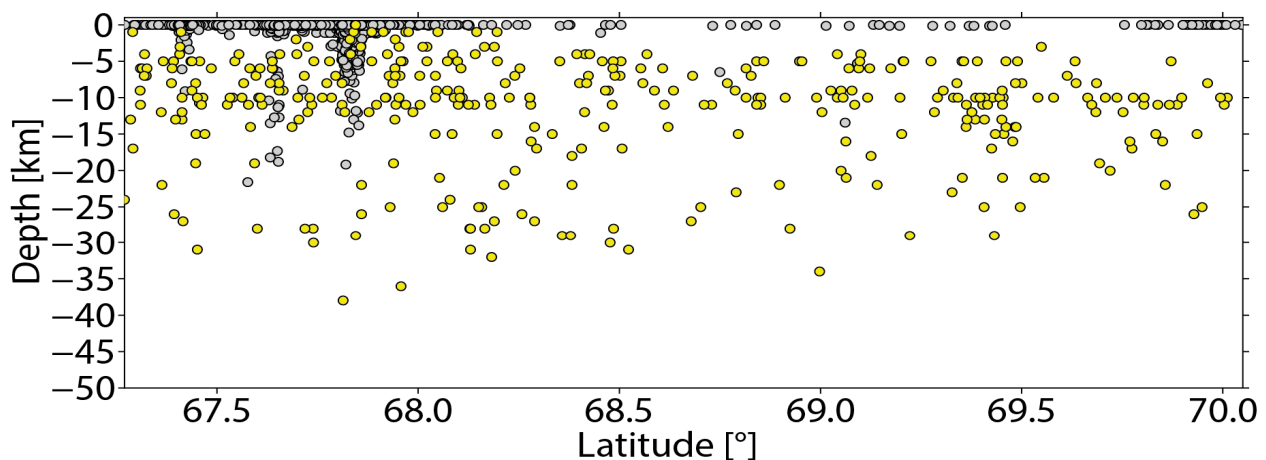


Figure 3. North–south distribution of seismicity along the PGFs intersected by the P0 profile in Figure 2. Yellow and gray dots represent earthquakes and explosions, induced and triggered events, respectively.

3.3. Preprocessing of Historical Seismic Data

The obtained dataset comes from a total of 46 stations (triangles in Figure 2), covering the period between the years 2007 and 2015. All the waveforms used in this study were downloaded in mseed format from different open data centers (GEOFON, IRIS, ORFEUS, RESIF, and UIB-NORSAR).

The coverage of seismological stations in the study area varies over time due to the installation of new stations in permanent networks (FN, HE, NO, NS, and UP) over the years and the existence of temporary networks (XK and 1G) (Table 1). The temporary network XK covered the southwestern zone of the network between the end of 2007 and 2009, and the network G1 covered the northeastern to southwestern zone of the faults between the end of 2012 and 2015. For the rest of the time, only permanent stations with a non-homogeneous distribution were available. Station coordinates and recording times of all considered networks can be found in Supplement S3.

The downloaded datasets were merged and transformed into SAC format using the ObsPy Python library [71]. This served as the input file for the autopicking program, discarding corrupted or non-readable data.

Table 1. Number of seismic stations per network with available open data downloaded in the study area, categorized by permanent and temporary stations, covering the period from 2007 to 2015.

	2007	2008	2009	2010	2011	2012	2013	2014	2015
Permanent Networks									
FN	1	1	1	1	1	1	1	1	1
HE	4	4	4	4	4	4	4	4	4
NO ¹	1	1	1	1	1	1	1	2	2
NS	2	2	2	2	3	3	3	3	3
UP	1	1	1	1	1	1	1	1	1
Sub-Total	9	9	9	9	10	10	10	11	11
Temporary Networks									
XK	19	19	19	0	0	0	0	0	0
1G	0	0	0	0	0	5	13	13	13
Sub-Total	19	19	19	0	0	5	13	13	13
Total of Stations	28	28	28	9	10	15	23	24	24

¹ NORSAR Station Network (NO) contains a 3 km aperture array of 26 stations. Due to the size of the study area, we only used 1 station: ARA0.

3.4. Making a New Earthquake Catalog

3.4.1. Automatic Earthquake Detection Code

Several types of automatic earthquake detection programs have been developed in academia and industry, designed to facilitate the processing of seismic records to identify and locate seismic events. Examples include STA/LTA (Short-Term Average/Long-Term Average) [72,73], waveform correlation [74], machine-learning-based methods [75,76], and autoregressive approaches [77], among others. These types of programs have been widely used for seismic monitoring, allowing us to update and/or generate new seismic catalogs.

To create the improved PGF earthquake catalog (hereafter referred as the “new catalog”), we generated a pre-catalog of potential seismic events by analyzing the downloaded and preprocessed seismic records using the Regressive ESTimator (REST) algorithm described in [78]. REST is a body wave arrival time autopicking program that uses autoregressive approaches to generate seismic event catalogs from existing seismic recordings, allowing a rapid analysis of large datasets. REST has been applied in various studies to create new catalogs and improve existing ones [79,80], including contexts such as cortical active faults [79], subduction zones [78,81–83], and mining exploration [84,85]. The REST process starts by analyzing the vertical -Z- components of the seismic traces for all available stations, performing automatic phase detection, and generating an onset file of potential P-wave picks. In the second step, the algorithm clusters these detections in time to generate a list of possible events using criteria based on station coverage and detection intervals. Finally, REST uses an iterative process based on [86,87] followed by data windowing procedures [88] to locate and filter the list of possible events: In the first step, events with P-wave arrival times are located. Once located, the predicted P-wave arrival times are calculated for all stations, and the P-wave onset estimates are redone using windows based on the predicted P-wave arrival times. This process is iterative. When a reasonable location is found, the second step is repeated, including the estimation of the S-wave arrival. In this way, a P- and S-wave onset plus event relocation is performed. If the location is again reasonable, the last step is repeated with more exhaustive criteria to define whether the onset corresponds to a cataloged event. The output file obtained with REST is a catalog of possible P- and S-wave arrival times associated with a seismic event, along with its location and time of origin. The program does not classify earthquake types or the source of origin.

3.4.2. Calibration of REST Parameters

Before running the REST algorithm on the entire dataset, we performed a calibration process to adjust the parameters of the algorithm to the specific seismic characteristics of the study area. This involved cutting time windows from SAC files for earthquakes listed in the FENCAT catalog and running REST on these windows several times. By analyzing the detection performance and adjusting the parameters accordingly, we optimized the algorithm's ability to distinguish seismic signals in this region.

The final calibration shows that the results are improved if the phase detection process is performed twice with two different filter ranges and the final result is merged into a single P-wave onset. In this case, a Bessel filter with a high-pass of 3 Hz and a low-pass at the Nyquist frequency was first applied, followed by a high-pass of 2 Hz and a low-pass of 4 Hz. Then, detections were clustered within 30 s for low station coverage and 10 s for high coverage, requiring at least 4 detections to mark a candidate event. For iterative relocation, we used the 1D velocity model presented in [89], and the process involved three steps: initial P-wave location, refined onset estimation using predicted windows, and incorporation of S-waves for final relocation.

The final criteria for a signal to be considered as a potential event for the pre-catalog were a minimum of 4 phases (3 P-waves and 1 S-wave) with less than a 1.2 s absolute travel time residual and a 5% relative travel time residual, and a maximum standard deviation of 1.5 s for all residuals, producing a pre-catalog with 25,046 potential seismic events.

3.4.3. Checking the Pre-Catalog

To verify the results of the pre-catalog of potential events centered on the PGF, we separated earthquakes associated with PGF zones from other seismic events in the study area by location:

- 1 Earthquakes associated with PGF zones: The earthquakes located in the zones associated with the PGFs were filtered by location and manually checked to improve the precision of the P-wave and S-wave arrival times. It is worth mentioning that this manual review was performed using the Bessel filter for better visualization, using bandwidths between 9 Hz and 4 Hz for a first revision of the events. Then, in necessary cases, bandwidths between 23 Hz and 3 Hz and between 4 Hz and 2 Hz were used to improve the P- and S-wave picks, respectively;
- 2 Events outside the PGF zones: Events outside the PGF zones were subjected to a more stringent filtering process to ensure data quality and accuracy. The filtering criteria were dynamically adjusted based on the number of seismic stations available at the time of each event and the minimum number of P- and S-wave phases required to be considered as a seismic event. These criteria are shown in Table 2.

Table 2. Minimum P-wave and S-wave phase criteria required for earthquake inclusion in the new catalog for events outside the PGF zone, based on the number of stations available at the time of the event.

N° of Stations Available	N° of P-Waves	N° of S-Waves
Up to 6	3	2
6–10	4	3
11–15	5	4
16–20	6	5
More than 20	7	6

3.4.4. Determining the Improved New Catalog

After a thorough filtering and manual review process, the pre-catalog obtained by REST was refined from 25,046 to 2179 events, achieving a reduction of approximately 92%. The locations of the remaining events were recalculated and the established criteria for

event validation were reapplied. The new catalog is composed of 2179 events, with a total of approximately 24,000 P-wave arrivals and 20,000 S-wave arrivals (see Supplement S4).

4. Results and Discussion

The final catalog of seismic events was classified into two distinct groups based on epicentral locations: events potentially related to the PGFs (indicated by yellow dots in Figure 4) and other seismic events (gray dots in Figure 4). This classification allows a clearer analysis of the seismic activity in the study area by distinguishing between tectonic and non-tectonic events, such as those induced by mining.

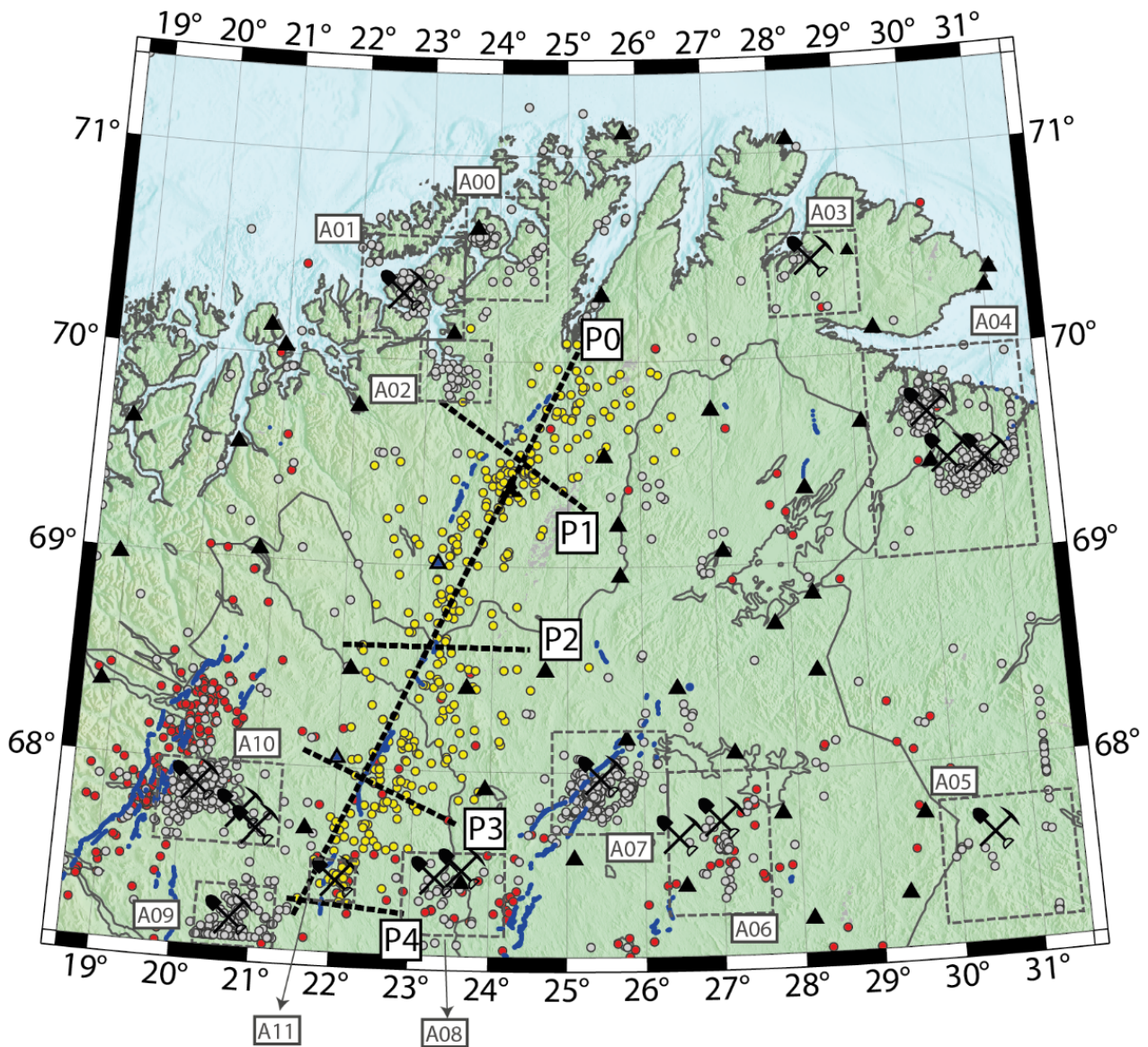


Figure 4. Map of the new earthquake catalog. Yellow dots represent earthquakes that may be associated with the PGFs present in the study area. Gray dots represent events outside the PGF zone picked by REST, and red dots represent FENCAT events that were not identified by REST. Black lines indicate the location of vertical profiles: P0 along the main strike of the fault systems, and P1 to P4 perpendicular to each fault system shown in Figure 5. In blue are the PGFs: SFC: Stuuragurra fault complex; PFS: Palojärvi fault system; LSFS: Lainio–Suijavaara fault system; MFS: Merasjärvi fault system. Triangles represent seismic stations. Shovel cross symbols represent active mines in the study area. Gray dotted line boxes represent the filter area for each mine.

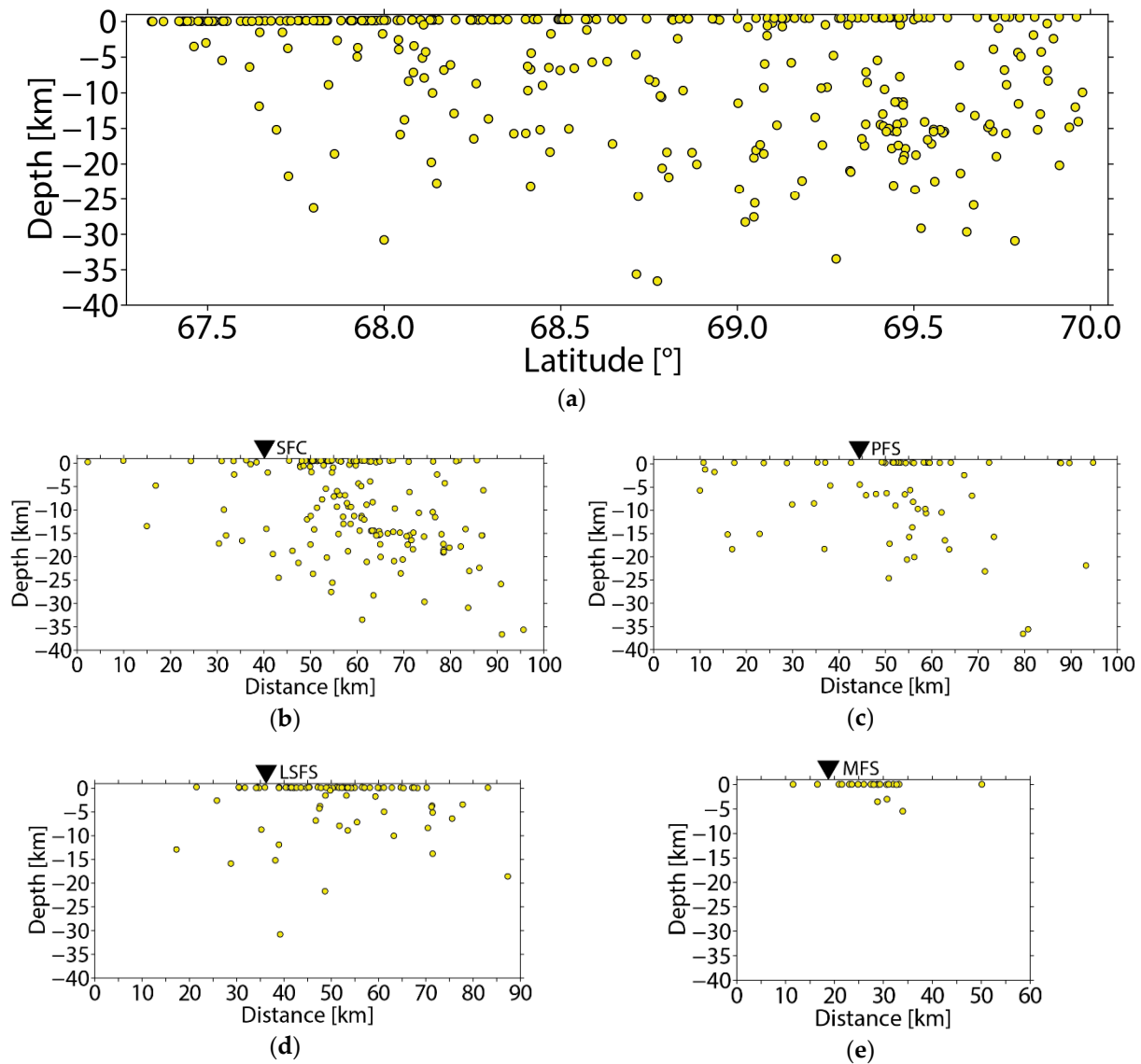


Figure 5. Seismicity along vertical profiles shown in Figure 4: (a) north–south distribution of seismicity along the PGFs, (b–e) vertical sections: Stuoragurra fault complex and Palojärvi, Lainio–Suijavaara, and Merasjärvi fault systems.

4.1. Comparative Analysis of the New Catalog and FENCAT

A comparative analysis between the new catalog and the FENCAT catalog revealed important differences in the detection of seismic events. In the new catalog, a total of 336 earthquakes are located within the PGF zones, while 1843 events occur outside these zones.

When focusing the comparison on PGFs' seismicity, one of the major improvements in the new catalog is the identification of 63 additional events within the PGF zones that were not captured in the FENCAT catalog, representing a 22% increase in detected relevant seismicity. However, 25 events listed in FENCAT were not captured in the new catalog by the autopicking process. This discrepancy highlights the potential limitations of automated detection methods, which may miss certain low-magnitude or complex events that require manual verification.

The temporal distribution of the events (Table 3) shows that of the 65 newly identified events, 78% occurred between 2007 and 2011, after which there is a decrease in the number of detected events. This decrease coincides with the installation of the HAMF station (part of the NS network) in 2011, located in the northern region of the PGF zone, a previously

poorly monitored area. The new station has likely improved detection capabilities in this region.

Table 3. Number of new events to be added in the new catalog compared to the FENCAT catalog per year.

Year	N° of New Events	%
2007	10	16%
2008	19	30%
2009	7	11%
2010	5	8%
2011	8	13%
2012	3	5%
2013	5	8%
2014	4	6%
2015	2	3%
TOTAL	63	100%

Analysis of the spatial distribution of the newly detected events (Table 4) shows that 49 are located in the Stuuragurra fault complex (SFC) zone, 4 in the Pärvie fault system (PFS), 3 in the Lainio–Suijjavaara fault system (LSFS), and 7 in the Merasjärvi fault system (MFS). Especially in the vicinity of the MFS zone, many of the shallow events are likely to be related to mining activity. Consequently, 14 of the 65 newly identified earthquakes are classified as potential explosions or induced events, with all new events in the MFS classified as mining-related.

Table 4. Number of new events to be added in the new catalog compared to the FENCAT catalog per PGFs.

PGFs	N° of New Events	%
SFC	49	78%
PFS	4	6%
LSFS	3	5%
MFS	7	11%

Of the total number of events outside the PGF zones, 1633 (approximately 89%) are clustered within identified mining zones. Based on their locations and frequency, this seismicity is likely related to mining activities, including explosive, induced, or triggered events. However, due to the presence of other postglacial faults in the area, such as the Pärvie and Suasselkä faults, which are close to active mines, the final classification as either tectonic or man-made must be made manually based on the characteristics of each earthquake. The new catalog fails to detect 259 earthquakes listed in FENCAT (red dots in Figure 4) outside the PGF zones, with most of these events concentrated in the southwestern part of the study area. This discrepancy is largely due to the sparse coverage of seismological stations with open data in this region throughout the study period. The detection gap underscores the critical role that a consistent monitoring network density plays in ensuring accurate seismic detection and event classification. A comparison between the number of events detected by REST outside the PGF zones and those not included in the FENCAT catalog was not made because FENCAT is filtered exclusively for tectonic earthquakes.

4.2. Seismicity from the Stuoragurra Fault Complex to the Merasjärvi Fault System

To better understand the spatial distribution of earthquakes from the SFC to the MFS, hypocenters were plotted in a map view and using 40 km depth vertical profiles, as shown in Figures 4 and 5, respectively.

As shown in Figure 4, the seismic events are spatially continuous from the SFC to the MFS. This is consistent with [42,45], which suggest the possibility of a deeper connection between the various SW-NE striking, thrusting PGF faults described in the area. However, a geophysical imaging study needs to be conducted to confirm this assertion. For now, we can only make this assumption based on the spatial locations of the earthquakes. In addition, Figure 5a shows the events' depth distribution. As expected, earthquakes are distributed in the first 25 km of the crust. However, some events are deeper, reaching depths corresponding to the regional Moho discontinuity. These events must be carefully reviewed; an explanation for them is beyond the results produced in this study.

When observing the vertical seismicity distribution for each profile (Figure 5b–e), it is possible to note that the area around the SFC and PFS shows higher seismicity rates than those associated with the LSFS and MFS. In this regard, there are no seismic events associated with the MFS in the new catalog.

During the manual review of earthquakes associated with the PGFs, it was observed that the waveforms of these earthquakes had similar shapes that corresponded to the specific fault system from which they originated, as detected by the network of available seismological stations. This similarity in waveform shapes suggests a distinct pattern associated with each fault system. Figure 6 shows representative examples of waveforms from each of the fault systems studied, providing a visual illustration of the consistent characteristics observed across different fault zones.

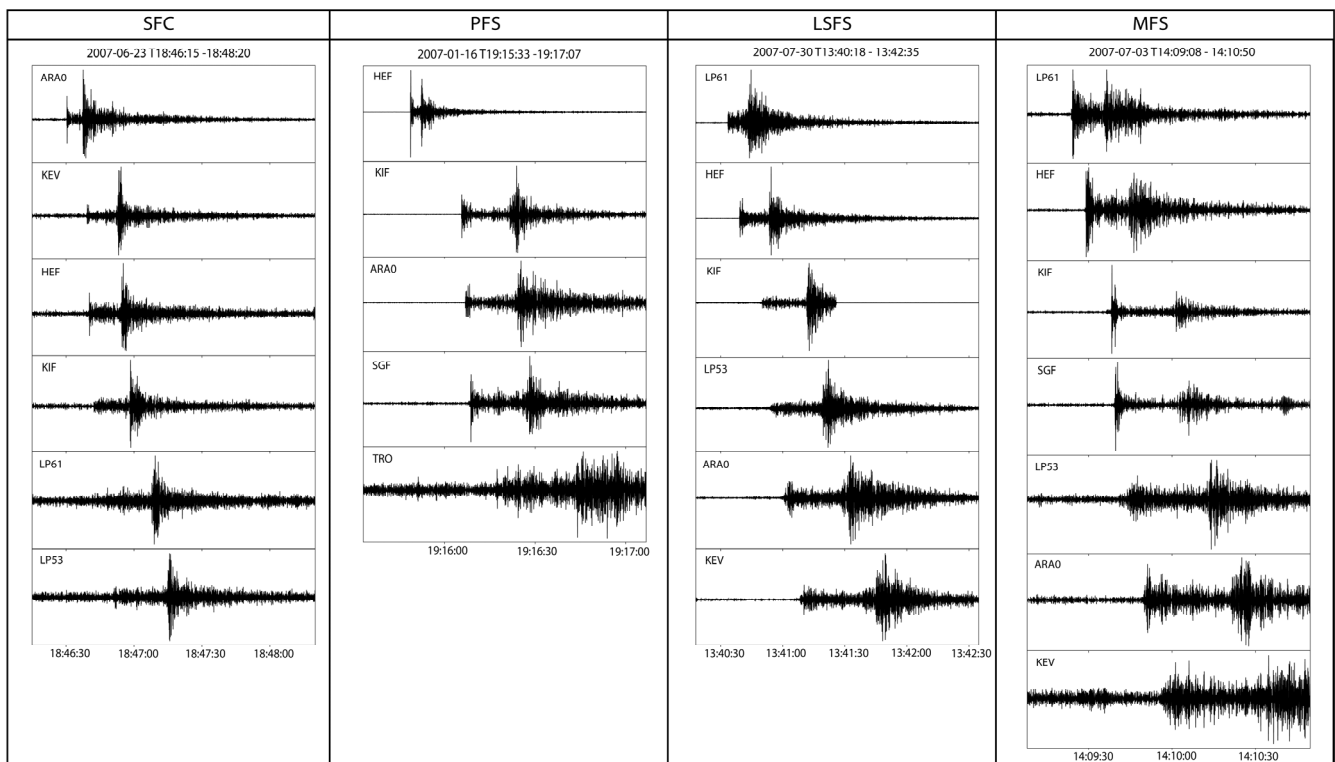


Figure 6. Examples of earthquake waveforms for each PGF. From left to right, SFC: Stuoragurra fault complex; PFS: Palojärvi fault system; LSFS: Lainio–Suijavaara fault system; MFS: Merasjärvi fault system. Figure shows the vertical component waveforms recorded at each station.

4.3. Seismicity of Mining Activity

Mining activities can generate a variety of seismic signals, both intentional and unintentional, due to the mechanical and explosive processes involved [90,91]. This type of seismicity accounts for a significant portion of the seismic signals recorded in Norway, Finland, and Sweden, largely exceeding tectonic events in both frequency and magnitude [53–55]. The seismic waveforms generated by mining activities typically have distinct characteristics that allow them to be distinguished from tectonic events. In our manual review process, we observed that the waveforms from mining events exhibited consistent patterns across different mining zones, regardless of the source location. Figure 7 shows a representative waveform example from each mining zone to illustrate the similarities in signal patterns that led to these reclassifications. This consistency was a key criterion for identifying and reclassifying several events as mining-related in our revised catalog.

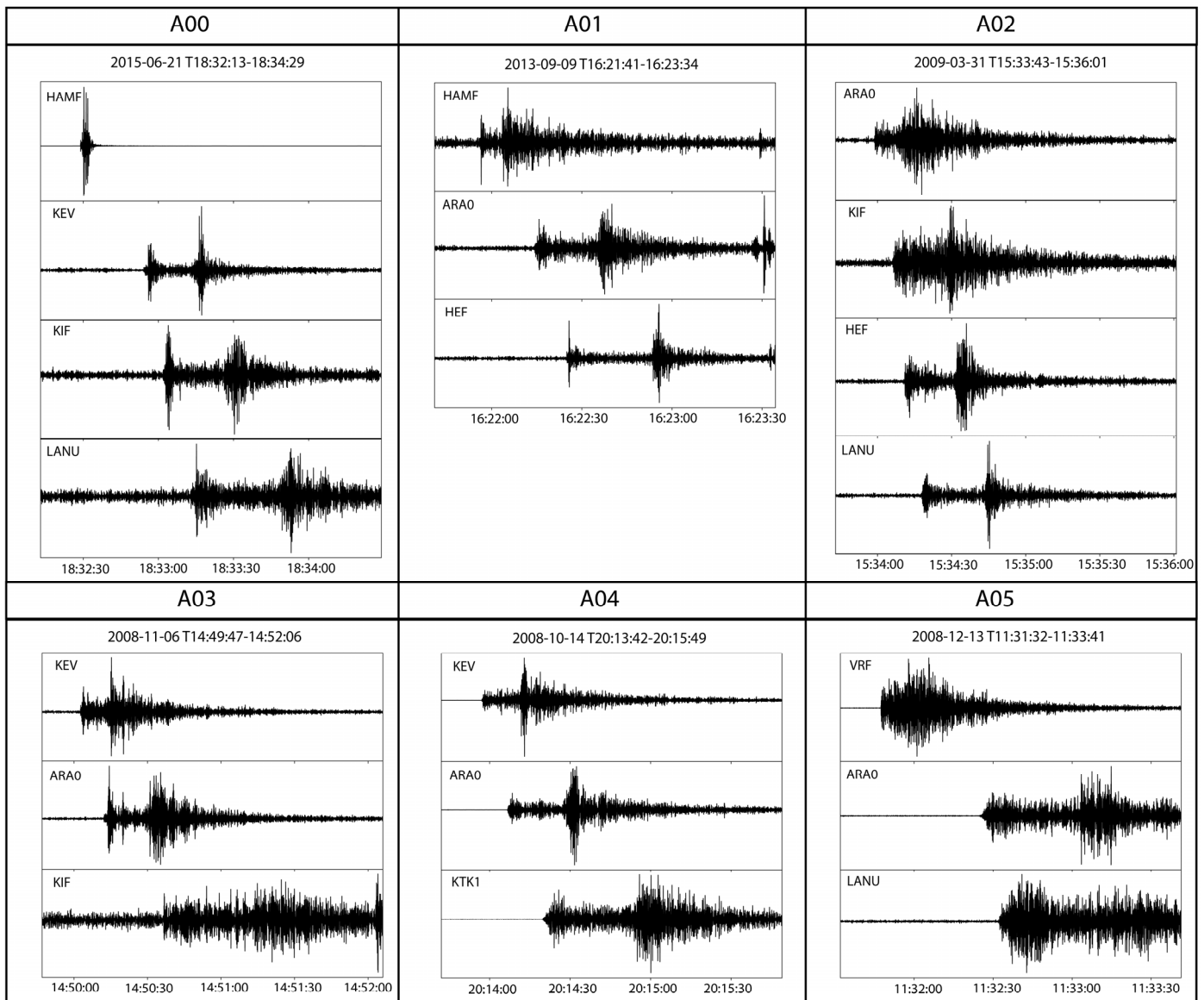


Figure 7. Cont.

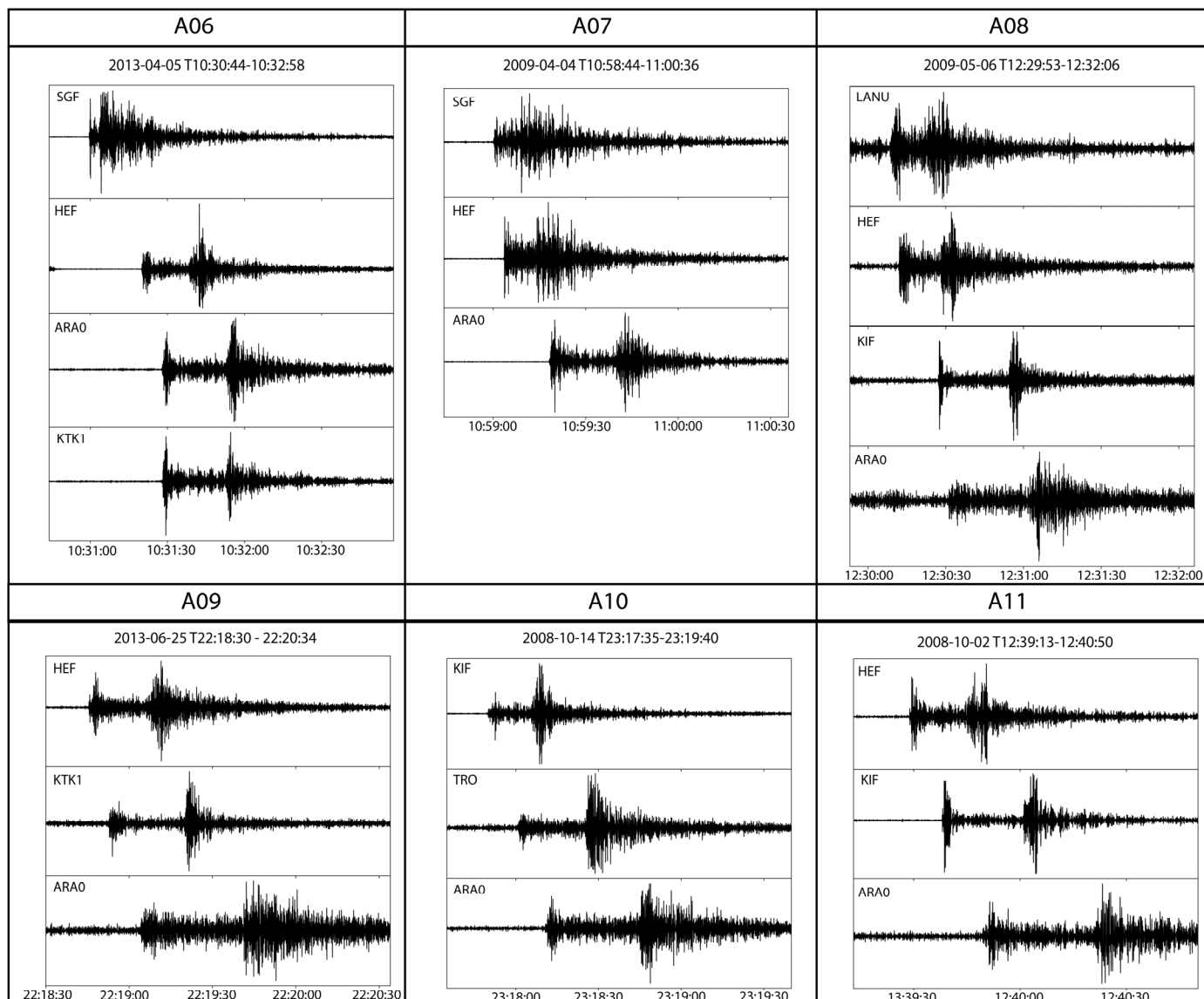


Figure 7. Example of waveforms detected in each of the mining zones delineated in Figure 4. The figure represents the vertical components.

5. Conclusions

This study highlights the importance of continuously updating and refining seismic catalogs, especially in regions of low tectonic seismicity such as northern Fennoscandia. The use of automated selection software such as REST, combined with rigorous manual verification, can significantly improve seismic datasets. This approach is particularly relevant in areas where traditional, purely human detection tends to miss a significant number of low-magnitude events.

The initial automated pre-catalog identified 25,046 potential seismic events. After extensive filtering and verification, 2179 of these events were considered eligible for inclusion in the new catalog, representing a 92% reduction. This significant reduction demonstrates the effectiveness of the process in removing noise, false positives, and irrelevant signals, thereby improving the reliability and accuracy of the seismic dataset. At the same time, this reduction can be translated into a software shortcoming, as its output needs to be carefully checked to catalog an earthquake.

One of the most significant improvements in the new catalog is the enhancement and improved identification of earthquakes within the postglacial fault (PGF) zones. The new catalog identifies 336 events within these zones compared to 285 in the FENCAT catalog,

representing a 26% increase. This increase is critical for studying intraplate seismicity and advancing the understanding of the tectonic activity associated with the PGFs. In contrast, outside the PGF zones, the new catalog records 1,843 events, of which approximately 89% are associated with known mining areas.

Compared to FENCAT, the new catalog shows a more precise differentiation between tectonic and mining events. FENCAT lists 407 events outside the PGF zones, of which only 28% are related to mining activities, highlighting the improved classification achieved in this study. However, the new catalog does not include 25 PGF-associated events and 259 events outside the PGF zones listed in FENCAT. These omissions are largely due to low-magnitude events with noisy signals, the sparse coverage of seismological stations in certain areas, and the challenge of tuning detection algorithms for a region characterized by diverse signal types, most of which are man-made.

Spatial analysis of the seismicity reveals a continuous cluster of earthquakes along the Merasjärvi, Lainio–Suijavaara, Palojärvi, and Maze and Iešjávri fault systems, extending to depths of up to 30 km. In particular, most events deeper than 5 km are concentrated between the Stuoragurra fault complex (SFC) and the Palojärvi fault system, while seismicity in the southern regions (LSFS and MFS) is predominantly shallow (~0 km depth). This spatial distribution suggests that these fault systems may be part of a larger, 300 km long deformation complex, which we propose naming the Merasjärvi–Stuoragurra fault complex.

Despite the advances in automated detection methods, distinguishing between tectonic and mining events remains a significant challenge due to the dominance of low-magnitude seismicity. In the Norwegian context, where natural tectonic activity is sparse and low-magnitude, mining signals can easily be misinterpreted as natural events. This challenge is exacerbated by the proximity of mining areas to fault zones, where tectonic and induced events may spatially overlap. Manual review remains necessary in many of these cases. The revised catalog addresses these ambiguities through detailed waveform analysis and event relocation. Key indicators such as P- and S-wave arrival patterns, frequency content, and event duration were instrumental in distinguishing the impulsive, high-frequency nature of mining explosions from the more complex waveforms of tectonic earthquakes.

It is proposed as future work that the catalog should be completed, including processing more years in the dataset, and that the catalog data should be used to obtain a 3D velocity model through local earthquake tomography. Our main goal will be to image the fault zone in order to unravel the seismic processes in the fault, which could help to estimate possible large earthquakes in the future. This work may facilitate the construction of a more complete structural analysis of the area. It is also proposed that a seismic monitoring network should be installed, focused on the study of PGFs.

Supplementary Materials: The following supporting information can be downloaded at <https://www.mdpi.com/article/10.3390/geosciences14110293/s1>, S1: FENCAT catalog of study area; S2: Bulletin report of NNSN and ISUH catalog of study area; S3: Station list; S4: New catalog.

Author Contributions: Conceptualization, C.P.-O.; methodology, D.C.-G.; software, S.R.; validation, D.C.-G.; formal analysis, D.C.-G.; investigation, D.C.-G. and C.P.-O.; resources, C.P.-O. and D.C.; data curation: D.C.-G. and A.E.; writing—original draft preparation, D.C.-G. and C.P.-O.; writing—review and editing, D.C.-G., C.P.-O., D.C., F.H. and O.O.; visualization, D.C.-G.; supervision, C.P.-O. and D.C.; project administration, C.P.-O.; funding acquisition, C.P.-O. and D.C. All authors have read and agreed to the published version of the manuscript.

Funding: This research was funded by the Norwegian Research Council through SINTEF, and the National Agency for Research and Development of Chile (ANID) by AFB180004, AFB220002, and AFB230001 projects.

Data Availability Statement: The original data presented in this study are openly available in the GEOFON Program (GEOFON) [<http://geofon.gfz-potsdam.de/fdsnws/dataselect/1/>]; Norwegian National Seismic Network (UIB-NORSAR) [<http://eida.geo.uib.no/fdsnws/dataselect/1/>]; The ORFEUS Data Center (ORFEUS) [<http://www.orfeus-eu.org/fdsnws/dataselect/1/>]; RESIF (RESIF) [<http://ws.resif.fr/fdsnws/dataselect/1/>]; and EarthScope Data Center (IRISDMC) [<http://service.iris.edu/fdsnws/dataselect/1/>]. Data from each source was accessed between September 2021 and October 2022.

Acknowledgments: Figures were constructed with the Generic Mapping Tools (GMT) data processing and display package (Wessel and Smith 1991, 1995). C.P.O. thanks the SEP project ‘Ambient Noise Tomography and Passive Seismicity for CO₂ imaging and monitoring’, funded by the Norwegian Research Council through SINTEF.

Conflicts of Interest: The authors declare no conflicts of interest.

References

1. Steffen, H.; Olesen, O.; Sutinen, R. *Glacially-Triggered Faulting*; Cambridge University Press: Cambridge, UK, 2021; ISBN 978-1-108-49002-3.
2. Wood, R.M. Extraordinary Deglaciation Reverse Faulting in Northern Fennoscandia. In *Earthquakes at North-Atlantic Passive Margins: Neotectonics and Postglacial Rebound*; Gregersen, S., Basham, P.W., Eds.; NATO ASI Series; Springer: Dordrecht, The Netherlands, 1989; pp. 141–173, ISBN 978-94-009-2311-9.51.
3. Olesen, O.; Henkel, H.; Lile, O.B.; Mairing, E.; Rønning, J.S. Geophysical Investigations of the Stuuragurra Postglacial Fault, Finnmark, Northern Norway. *J. Appl. Geophys.* **1992**, *29*, 95–118. [[CrossRef](#)]
4. Olesen, O.; Bungum, H.; Dehls, J.; Lindholm, C.; Pascal, C.; Roberts, D. Neotectonics, Seismicity and Contemporary Stress Field in Norway—Mechanisms and Implications. *Geol. Surv. Nor. Spec. Publ.* **2013**, *13*, 145–174.
5. Dehls, J.F.; Olesen, O.; Olsen, L.; Harald Blikra, L. Neotectonic Faulting in Northern Norway; the Stuuragurra and Nordmannvikdalen Postglacial Faults. *Quat. Sci. Rev.* **2000**, *19*, 1447–1460. [[CrossRef](#)]
6. Mörrer, N.A. Active faults and paleoseismicity in Fennoscandia, especially Sweden. Primary structures and secondary effects. *Tectonophysics* **2004**, *380*, 139–157. [[CrossRef](#)]
7. Mikko, H.; Smith, C.A.; Lund, B.; Ask, M.V.S.; Munier, R. LiDAR-Derived Inventory of Post-Glacial Fault Scarps in Sweden. *GFF* **2015**, *137*, 334–338. [[CrossRef](#)]
8. Berglund, M.; Dahlström, N. Post-Glacial Fault Scarps in Jämtland, Central Sweden. *GFF* **2015**, *137*, 339–343. [[CrossRef](#)]
9. Smith, C.A.; Griggull, S.; Mikko, H. Geomorphic Evidence of Multiple Surface Ruptures of the Merasjärvi “Postglacial Fault”, Northern Sweden. *GFF* **2018**, *140*, 318–322. [[CrossRef](#)]
10. Olsen, L.; Olesen, O.; Dehls, J.; Tassis, G.A. Late-/Postglacial Age and Tectonic Origin of the Nordmannvikdalen Fault, Northern Norway. *Nor. J. Geol.* **2019**, *98*, 483–500. [[CrossRef](#)]
11. Mattila, J.; Ojala, A.E.K.; Ruskeeniemi, T.; Palmu, J.-P.; Aaltonen, I.; Käpyaho, A.; Lindberg, A.; Sutinen, R. Evidence of Multiple Slip Events on Postglacial Faults in Northern Fennoscandia. *Quat. Sci. Rev.* **2019**, *215*, 242–252. [[CrossRef](#)]
12. Brandes, C.; Steffen, H.; Sandersen, P.B.E.; Wu, P.; Winsemann, J. Glacially Induced Faulting along the NW Segment of the Sorgenfrei-Tornquist Zone, Northern Denmark: Implications for Neotectonics and Lateglacial Fault-Bound Basin Formation. *Quat. Sci. Rev.* **2018**, *189*, 149–168. [[CrossRef](#)]
13. Gregersen, S.; Voss, P.H. Review of Some Significant Claimed Irregularities in Scandinavian Postglacial Uplift on Timescales of Tens to Thousands of Years—Earthquakes in Denmark? *Solid Earth* **2014**, *5*, 109–118. [[CrossRef](#)]
14. Stewart, I.S.; Sauber, J.; Rose, J. Glacio-Seismotectonics: Ice Sheets, Crustal Deformation and Seismicity. *Quat. Sci. Rev.* **2000**, *19*, 1367–1389. [[CrossRef](#)]
15. Reicherter, K.; Kaiser, A.; Stackebrandt, W. The Post-Glacial Landscape Evolution of the North German Basin: Morphology, Neotectonics and Crustal Deformation. *Int. J. Earth Sci. (Geol. Rundsch.)* **2005**, *94*, 1083–1093. [[CrossRef](#)]
16. Grube, A. Palaeoseismic Structures in Quaternary Sediments of Hamburg (NW Germany), Earthquake Evidence during the Younger Weichselian and Holocene. *Int. J. Earth Sci. (Geol. Rundsch.)* **2019**, *108*, 845–861. [[CrossRef](#)]
17. Brodzikowski, K. Pleistocene Glacigenic Deposition in a Tectonically Active, Subsiding Zone: The Kleszczów Graben, Central Poland. In *Glacial Deposits in Northeast Europe*; Ehlers, J., Kozarski, S., Gibbard, P.L., Eds.; CRC Press: Rotterdam, The Netherlands, 1995; pp. 361–385, ISBN 978-1-00-307769-5.
18. Pisarska-Jamróży, M.; Van Loon, A.J.; Mleczak, M.; Roman, M. Enigmatic Gravity-Flow Deposits at Ujście (Western Poland), Triggered by Earthquakes (as Evidenced by Seismites) Caused by Saalian Glacioisostatic Crustal Rebound. *Geomorphology* **2019**, *326*, 239–251. [[CrossRef](#)]
19. Brooks, G.R.; Adams, J. A Review of Evidence of Glacially-Induced Faulting and Seismic Shaking in Eastern Canada. *Quat. Sci. Rev.* **2020**, *228*, 106070. [[CrossRef](#)]
20. Ma, S.; Eaton, D.W.; Adams, J. Intraplate Seismicity of a Recently Deglaciated Shield Terrane: A Case Study from Northern Ontario, Canada. *Bull. Seism. Soc. Am.* **2008**, *98*, 2828–2848. [[CrossRef](#)]

21. Sauber, J.; Ruppert, N. Rapid Ice Mass Loss: Does It Have an Influence on Earthquake Occurrence in Southern Alaska? In *Active Tectonics and Seismic Potential of Alaska*; Freymueller, J., Haeussler, P., Wesson, R., Ekström, G., Eds.; Geophysical Monograph Series; John Wiley & Sons: Hoboken, NJ, USA, 2008; Volume 179.
22. Koehler, R.D.; Carver, G.A.; Alaska Seismic Hazards Safety Commission. Active faults and seismic hazards in Alaska. *Alsk. Div. Geol. Geophys. Surv. Misc. Publ.* **2018**, *160*, 59. [[CrossRef](#)]
23. Bungum, H.; Lindholm, C. Seismo- and Neotectonics in Finnmark, Kola and the Southern Barents Sea, Part 2: Seismological Analysis and Seismotectonics. *Tectonophysics* **1997**, *270*, 15–28. [[CrossRef](#)]
24. Olesen, O.; Olsen, L.; Gibbons, S.J.; Ruud, B.O.; Høgaas, F.; Johansen, T.A.; Kværna, T. Postglacial Faulting in Norway: Large Magnitude Earthquakes of the Late Holocene Age. In *Glacially-Triggered Faulting*; Steffen, H., Olesen, O., Sutinen, R., Eds.; Cambridge University Press: Cambridge, UK, 2021; pp. 198–217, ISBN 978-1-108-49002-3.
25. Lund, B.; Roberts, R.; Smith, C. *Review of Paleo-, Historical and Current Seismicity in Sweden and Surrounding Areas with Implications for the Seismic Analysis Underlying SKI Report 92:3*; Swedish Radiation Safety Authority: Stockholm, Sweden, 2017; p. 62.
26. Ojala, A.E.K.; Markovaara-Koivisto, M.; Middleton, M.; Ruskeeniemi, T.; Mattila, J.; Sutinen, R. Dating of Paleolandslides in Western Finnish Lapland. *Earth Surf. Process. Landf.* **2018**, *43*, 2449–2462. [[CrossRef](#)]
27. Olsen, L.; Olesen, O.; Høgaas, F.; Poliakova, A.; Schönenberger, J.; van der Lelij, R.; Tassis, G.; Bjørlykke, A. *Trenching and 14C Dating of the Stuoragurra Fault Complex in Finnmark, Northern Norway—With Some Accompanying Data Included*; Geological Survey of Norway: Trondheim, Norway, 2022; p. 71.
28. Schurr, B.; Rietbrock, A. Deep seismic structure of the Atacama basin, northern Chile. *Geophys. Res. Lett.* **2004**, *31*, 12. [[CrossRef](#)]
29. Gibowicz, J. Seismicity induced by mining: Recent research. *Adv. Geophys.* **2009**, *51*, 1–53. [[CrossRef](#)]
30. Eilu, P.; Boyd, R.; Hallberg, A.; Korsakova, M.; Krasotkin, S.; Nurmi, P.; Ripa, M.; Stromov, V.; Tontti, M. Mining History of Fennoscandia. In *Mineral Deposits and Metallogeny of Fennoscandia*; Eilu, P., Ed.; Special Paper 53; Geological Survey of Finland: Espoo, Finland, 2012; Volume 2012, pp. 19–32.
31. Mörner, N.A. Past and present uplift in Sweden: Glacial isostasy, tectonism and bedrock influence. *Geol. Foereningen Stock. Foerhandlingar* **1977**, *99*, 48–54. [[CrossRef](#)]
32. Mörner, N.A. Faulting, fracturing, and seismicity as functions of glacio-isostasy in Fennoscandia. *Geol. J.* **1978**, *6*, 41–45. [[CrossRef](#)]
33. Mörner, N.A. Paleoseismicity and geodynamics in Sweden. *Tectonophysics* **1984**, *117*, 139–153. [[CrossRef](#)]
34. Lund, B.; Schmidt, P.; Hieronymus, C. *Stress Evolution and Fault Stability During the Weichselian Glacial Cycle*; Technical Report TR-09-15 19; Swedish Nuclear Fuel and Waste Management Co. (SKB): Stockholm, Sweden, 2009.
35. Dumais, M.A.; Olesen, O.; Gernigon, L.; Johansen, S.; Brønner, M. Delineating the Geological Settings of the Southern Fram Strait with State-of-the-Art Aeromagnetic Data. In Proceedings of the 34th Nordic Geological Winter Meeting, Oslo, Norway, 8–10 January 2020; p. 51.
36. Olesen, O. The Stuoragurra Fault, Evidence of Neotectonics in the Precambrian of Finnmark, Northern Norway. *Nor. Geol. Tidsskr.* **1988**, *68*, 107–119.
37. Bungum, H.; Fyen, J. Hypocentral Distribution, Focal Mechanisms, and Tectonic Implications of Fennoscandian Earthquakes, 1954–1978. *Geol. Foereningen Stock. Foerhandlingar* **1980**, *101*, 261–271. [[CrossRef](#)]
38. Gradmann, S.; Olesen, O.; Keiding, M.; Maystrenko, Y. The Regional 3D Stress Field of Nordland, Northern Norway—Insights from Numerical Modelling. In *Neotectonics in Nordland—Implications for Petroleum Exploration (NEONOR2)*; Geological Survey of Norway: Trondheim, Norway, 2018; pp. 215–240.
39. Gradmann, S.; Keiding, M.; Olesen, O.; Maystrenko, Y. The 3D Stress Field of Nordland, Northern Norway—Insights from Numerical Modelling. In Proceedings of the EGU General Assembly 2023, Vienna, Austria, 24 April 2023; Volume EGU23-13955.10.
40. Stephansson, O.; Sarkka, P.; Myrvang, A.; Hansen, T.H.; Vaatliinen, A.; Dahlstrom, L.O.; Bergstrom, K.; Fjeld, O.K. *Fennoscandian Rock Stress Data Base—FRSDB*; Luleå Tekniska Universitet: Luleå, Sweden, 1987.
41. Olesen, O.; Blikra, L.; Braathen, A.; Dehls, J.; Olsen, L.; Rise, L.; Roberts, D.; Riis, F.; Faleide, J.I.; Anda, E. Neotectonic Deformation in Norway and Its Implications: A Review. *Nor. J. Geol./Nor. Geol. Foren.* **2004**, *84*, 3–34.
42. Lagerbäck, R.; Sundh, M. *Early Holocene Faulting and Paleoseismicity in Northern Sweden*; Sveriges Geologiska Undersökning—Research Paper: Uppsala, Sweden, 2008; Volume 836.
43. Munier, R.; Adams, J.; Brandes, C.; Brooks, G.; Dehls, J.; Einarsson, P.; Gibbons, S.J.; Hjartardóttir, Á.R.; Høgaas, F.; Johansen, T.A.; et al. International Database of Glacially Induced Faults. PANGAEA. 2020. Available online: <https://doi.pangaea.de/10.1594/PANGAEA.922705> (accessed on 5 November 2021). [[CrossRef](#)]
44. Bungum, H.; Lindholm, C.D.; Dahle, A.; Woo, G.; Nadim, F.; Holme, J.K.; Gudmestad, O.T.; Hagberg, T.; Karthigeyan, K. New Seismic Zoning Maps for Norway, the North Sea, and the United Kingdom. *Seism. Res. Lett.* **2000**, *71*, 687–697. [[CrossRef](#)]
45. Sutinen, R.; Hyvönen, E.; Middleton, M.; Ruskeeniemi, T. Airborne LiDAR Detection of Postglacial Faults and Pulju Moraine in Palojärvi, Finnish Lapland. *Glob. Planet Change* **2014**, *115*, 24–32. [[CrossRef](#)]
46. Ojala, A.E.K.; Mattila, J.; Markovaara-Koivisto, M.; Ruskeeniemi, T.; Palmu, J.-P.; Sutinen, R. Distribution and Morphology of Landslides in Northern Finland: An Analysis of Postglacial Seismic Activity. *Geomorphology* **2019**, *326*, 190–201. [[CrossRef](#)]
47. Lagerbäck, R. Neotectonic Structures in Northern Sweden. *Geol. Foereningen Stock. Foerhandlingar* **1978**, *100*, 263–269. [[CrossRef](#)]

48. Olsen, L.; Olesen, O. Age and Associated Earthquake Magnitude of the Stuuragurra Fault Complex in Finnmark, Northern Norway. In Proceedings of the Vinterkonferansen 2023, 35th Geological Winter Meeting, Trondheim, Norway, 4–6 January 2023; Nakrem, H.A., Husås, A.M., Eds.; Abstracts and Proceedings of the Geological Society of Norway 1: Trondheim, Norway, 2023; p. 72.
49. Wells, D.L.; Coppersmith, K.J. New Empirical Relationships among Magnitude, Rupture Length, Rupture Width, Rupture Area, and Surface Displacement. *Bull. Seismol. Soc. Am.* **1994**, *84*, 974–1002. [CrossRef]
50. Smith, C.A.; Mikko, H.; Grigull, S. Glacially Induced Faults in Sweden: The Rise and Reassessment of the Single-Rupture Hypothesis. In *Glacially-Triggered Faulting*; Steffen, H., Olesen, O., Sutinen, R., Eds.; Cambridge University Press: Cambridge, UK, 2021; pp. 218–230, ISBN 978-1-108-49002-3.
51. Lagerbäck, R. *Postglacial Faulting and Paleoseismicity in the Lansjarv Area, Northern Sweden*; SKB Technical Report 88-25; Swedish Nuclear Fuel and Waste Management Co.: Stockholm, Sweden, 1988; 37p.
52. University of Helsinki, Institute of Seismology Website. Earthquake Search Tool. Available online: <https://www.seismo.helsinki.fi/EQ-search/query.php> (accessed on 24 August 2024).
53. Norwegian National Seismic Network Website. Seismic Catalogue. Available online: <https://nnsn.geo.uib.no/nnsn/#/data/events/search> (accessed on 24 August 2024).
54. University of Helsinki, Institute of Seismology Website. Final Monthly Bulletins. Available online: <https://www.helsinki.fi/en/institute-seismology/research/seismic-bulletins#analyst-reviewed-bulletins> (accessed on 24 August 2024).
55. Lund, B.; Schmidt, P.; Shomali, Z.; Roth, M. The Modern Swedish National Seismic Network: Two Decades of Intraplate Microseismic Observation. *Seism. Res. Lett.* **2021**, *92*, 1747–1758. [CrossRef]
56. Olesen, O.; Blikra, L.H.; Bockmann, L.; Bungum, H.; Dehls, J.F.; Faleide, J.I.; Fjeldskaar, W.; Hicks, E.; Lindholm, C.; Longva, O.; et al. *Neotectonics in Norway, Final Report*; Norges Geologiske Undersøkelse Report 2000.002; Geological Survey of Norway: Trondheim, Norway, 2000; Volume 135, p. 26.
57. Munier, R.; Fenton, C. Current Understanding and Directions for Future Studies—Review of Postglacial Faulting. In *Respect Distances—Rationale and Means of Computation*; Swedish Nuclear Fuel and Waste Management Co. (SKB): Stockholm, Sweden, 2004; Appendix 3.
58. Lindblom, E.; Lund, B.; Tryggvason, A.; Uski, M.; Bödvarsson, R.; Juhlin, C.; Roberts, R. Microearthquakes Illuminate the Deep Structure of the Endglacial Pärvie Fault, Northern Sweden. *Geophys. J. Int.* **2015**, *201*, 1704–1716. [CrossRef]
59. Ahmadi, O.; Juhlin, C.; Ask, M.; Lund, B. Revealing the Deeper Structure of the End-Glacial Pärvie Fault System in Northern Sweden by Seismic Reflection Profiling. *Solid Earth* **2015**, *6*, 621–632. [CrossRef]
60. Kukkonen, I.; Olesen, O.; Ask, M. Postglacial Faults in Fennoscandia: Targets for Scientific Drilling. *Geol. Foerhandlingar* **2010**, *132*, 71–81. [CrossRef]
61. Lindblom, E. Microearthquake Study of End-Glacial Faults in Northern Sweden. Ph.D. Dissertation, Uppsala University, Uppsala, Sweden, 2011.
62. SAGE. Seismological Facility for the Advancement of Geoscience Website, IRIS Map. Available online: https://ds.iris.edu/gmap/#starttime=2006-01-01&endtime=2024-08-31&maxlat=71.4&maxlon=31.5&minlat=66.4&minlon=16.2&network=*&drawingmode=box&planet=earth (accessed on 24 August 2024).
63. Sodankylä Geophysical Observatory/University of Oulu (Finland). *Northern Finland Seismological Network [Data Set]*; GFZ Data Services: Potsdam, Germany, 1980. [CrossRef]
64. Institute of Seismology. *The Finnish National Seismic Network [Data Set]*; GFZ Data Services: Potsdam, Germany, 1980. [CrossRef]
65. NORSAR. *NORSAR Station Network (NORSAR) [Data Set]*; NORSAR: Kjeller, Norway, 1971. [CrossRef]
66. University of Bergen. *University of Bergen Seismic Network [Data Set]*; University of Bergen: Bergen, Norway, 1982. [CrossRef]
67. SNSN. *Swedish National Seismic Network [Data Set]*; Uppsala University: Uppsala, Sweden, 1904. [CrossRef]
68. Silvennoinen, H.; Kozlovskaya, E.; Kissling, E. POLENET/LAPNET teleseismic *P* wave travel time tomography model of the upper mantle beneath northern Fennoscandia. *Solid Earth* **2016**, *7*, 425–439. [CrossRef]
69. Thybo, H.; Balling, N.; Maupin, V.; Ritter, J.; Tilmann, F. ScanArray Core (1G 2012–2017). The ScanArray Consortium. 2012. Available online: <https://geofon.gfz-potsdam.de/doi/network/1G/2012> (accessed on 24 August 2024).
70. GTK. Geological Survey of Finland Website, Fennoscandian Mineral Deposits. 2024. Available online: <https://gtkdata.gtk.fi/fmd/> (accessed on 24 August 2024).
71. Beyreuther, M.; Barsch, R.; Krischer, L.; Megies, T.; Behr, Y.; Wassermann, J. ObsPy: A Python Toolbox for Seismology. *Seism. Res. Lett.* **2010**, *81*, 530–533. [CrossRef]
72. Vaezi, Y.; Van der Baan, M. Comparison of the STA/LTA and power spectral density methods for microseismic event detection. *Geophys. J. Int.* **2015**, *203*, 1896–1908. [CrossRef]
73. Khalqillah, A.; Isa, M.; Muksin, U. A GUI based automatic detection of seismic P-wave arrivals by using Short Term Average/Long Term Average (STA/LTA) method. *J. Phys. Conf. Ser.* **2019**, *1116*, 032014. [CrossRef]
74. Gibbons, S.; Ringdal, F. The detection of low magnitude seismic events using array-based waveform correlation. *Geophys. J. Int.* **2016**, *165*, 149–166. [CrossRef]
75. Asim, K.M.; Martínez-Álvarez, F.; Basit, A.; Iqbal, T. Earthquake magnitude prediction in Hindukush region using machine learning techniques. *Nat. Hazards* **2017**, *85*, 471–486. [CrossRef]

76. Khan, I.; Choi, S.; Kwon, Y.-W. Earthquake Detection in a Static and Dynamic Environment Using Supervised Machine Learning and a Novel Feature Extraction Method. *Sensors* **2020**, *20*, 800. [[CrossRef](#)]
77. Takanami, T. A study of detection and extraction methods for microearthquake waves by autoregressive models. *J. Fac. Sci. Hokkaido University. Ser. 7 Geophys.* **1991**, *9*, 67–196.
78. Comte, D.; Farias, M.; Roecker, S.; Russo, R. The Nature of the Subduction Wedge in an Erosive Margin: Insights from the Analysis of Aftershocks of the 2015 Mw 8.3 Illapel Earthquake beneath the Chilean Coastal Range. *Earth Planet Sci. Lett.* **2019**, *520*, 50–62. [[CrossRef](#)]
79. Calle-Gardella, D.; Comte, D.; Fariás, M.; Roecker, S.; Rietbrock, A. Three-Dimensional Local Earthquake Tomography of Pre-Cenozoic Structures in the Coastal Margin of Central Chile: Pichilemu Fault System. *J. Seism.* **2021**, *25*, 521–533. [[CrossRef](#)]
80. Littel, G.F.; Bostock, M.G.; Schaeffer, A.; Roecker, S. Microplate Evolution in the Queen Charlotte Triple Junction & Explorer Region: New Insights From Microseismicity. *Tectonics* **2023**, *42*, e2022TC007494. [[CrossRef](#)]
81. Navarro-Aranguiz, A.; Comte, D.; Fariás, M.; Roecker, S.; Calle-Gardella, D.; Zhang, H.; Gao, L.; Rietbrock, A. Subduction Erosion and Basal Accretion in the Central Chile Subduction Wedge Inferred from Local Earthquake Tomography. *J. S. Am. Earth Sci.* **2022**, *115*, 103765. [[CrossRef](#)]
82. Yarce, J.; Sheehan, A.F.; Roecker, S. Temporal Relationship of Slow Slip Events and Microearthquake Seismicity: Insights From Earthquake Automatic Detections in the Northern Hikurangi Margin, Aotearoa New Zealand. *Geochem. Geophys. Geosyst.* **2023**, *24*, e2022GC010537. [[CrossRef](#)]
83. Leon-Rios, S.; Reyes-Wagner, V.; Calle-Gardella, D.; Rietbrock, A.; Roecker, S.; Maksymowicz, A.; Comte, D. Structural Characterization of the Taltal Segment in Northern Chile Between 22°S and 26°S Using Local Earthquake Tomography. *Geochem. Geophys. Geosyst.* **2024**, *25*, e2023GC011197. [[CrossRef](#)]
84. Bugueño, F.; Calle-Gardella, D.; Comte, D.; Reyes-Wagner, V.; Ojeda, M.; Rietbrock, A.; Roecker, S. Subsurface Insights of the Maricunga Gold Belt through Local Earthquake Tomography. *Minerals* **2022**, *12*, 1437. [[CrossRef](#)]
85. Comte, D.; Fariás, M.; Calle-Gardella, D.; Navarro-Aranguiz, A.; Roecker, S.; Rietbrock, A. Anomalous Intraslab Structure Revealed by the Analysis of Aftershocks of the Mw 6.7 Coquimbo-La Serena Earthquake of 20 January 2019. *Tectonophysics* **2023**, *846*, 229660. [[CrossRef](#)]
86. Pisarenko, V.F.; Kushnir, A.F.; Savin, I.V. Statistical Adaptive Algorithms for Estimation of Onset Moments of Seismic Phases. *Phys. Earth Planet Inter.* **1987**, *47*, 4–10. [[CrossRef](#)]
87. Kushnir, A.F.; Lapshin, V.M.; Pinsky, V.I.; Fyen, J. Statistically Optimal Event Detection Using Small Array Data. *Bull. Seism. Soc. Am.* **1990**, *80*, 1934–1950. [[CrossRef](#)]
88. Rawles, C.; Thurber, C. A Non-Parametric Method for Automatic Determination of P-Wave and S-Wave Arrival Times: Application to Local Micro Earthquakes. *Geophys. J. Int.* **2015**, *202*, 1164–1179. [[CrossRef](#)]
89. Havskov, J.; Bungum, H. Source Parameters for Earthquakes in the Northern North Sea. *NJG* **1987**, *67*, 51–58.
90. Cokk, N.G.W. Seismicity associated with mining. *Eng. Geol.* **1976**, *10*, 99–122. [[CrossRef](#)]
91. Gibowickz, S.; Kijko, A. *An Introduction to Mining Seismology*; Elsevier: San Diego, CA, USA, 1994; ISBN 978-0-08-091836-51994.

Disclaimer/Publisher’s Note: The statements, opinions and data contained in all publications are solely those of the individual author(s) and contributor(s) and not of MDPI and/or the editor(s). MDPI and/or the editor(s) disclaim responsibility for any injury to people or property resulting from any ideas, methods, instructions or products referred to in the content.